IOP Publishing Journal of Physics: Conference Series **59** (2007) 249–254
doi:10.1088/1742-6596/59/1/053 Eighth International Conference on Laser Ablation

Mechanisms of femtosecond laser nanoprocessing of biological cells and tissues

Alfred Vogel[1], Joachim Noack[1], Gereon Hüttmann[1] and Günther Paltauf[2]

[1] Biomedizinische Optik, Universität zu Lübeck, Peter-Monnik Weg 4, 23562 Lübeck, Germany

[2] Institut für Physik, Karl-Franzens-Universität, Universitätsplatz 5, A-8010 Graz, Austria

Abstract. We investigated the working mechanisms of femtosecond laser nanoprocessing in biomaterials with oscillator pulses of 80 MHz repetition rate and with amplified pulses of 1 kHz repetition rate. Plasma formation in water, the evolution of the temperature distribution, thermoelastic stress generation, and stress-induced cavitation bubble formation were numerically simulated for NA = 1.3 and the outcome compared to experimental results. A comparison of the thresholds for the various physical effects with experimental parameters enables to assess the working mechanisms of both modalities for cell surgery.

Nonlinear absorption of short and ultrashort laser pulses focused through microscope objectives of high numerical aperture (NA) can be used to achieve very fine and highly localized laser effects inside of biological media that are transparent at low irradiance as well as in the bulk of photonic materials [1]. Very large numerical apertures are required both to minimize the diffraction limited focus diameter and to avoid self-focusing and filamentation.

To make use of the full potential of femtosecond pulses for highly localized material processing and modification of biological media, it is essential to understand the underlying mechanisms. We have therefore investigated the evolution of plasma formation and the chemical, thermal, and thermomechanical effects arising from femtosecond optical breakdown in aqueous media. Details about the numerical and experimental methods applied in this study can be found in Ref [1].

While nanosecond breakdown is very abrupt (Figs. 1a, c), we find that in femtosecond laser optical breakdown free electrons are produced in a fairly large irradiance range below the optical breakdown threshold, with a deterministic relationship between free electron density and irradiance (Figs 1b, d). This provides a large 'tuning range' for the creation of spatially confined chemical, thermal and mechanical effects via free electron generation that can be used for cell surgery. The prediction of low-density plasmas at irradiances below the threshold for cavity formation (Fig. 1d) was experimentally confirmed by Mao et. al. [2]. For larger irradiances, plasmas in bulk media grow beyond the region of the beam waist, which keeps the plasma energy density small. By contrast, at surfaces the energy deposition becomes confined to a thin, dense layer once the free electron density reaches the critical density [3, 4], and the regime of low-density plasmas generation has little practical importance.

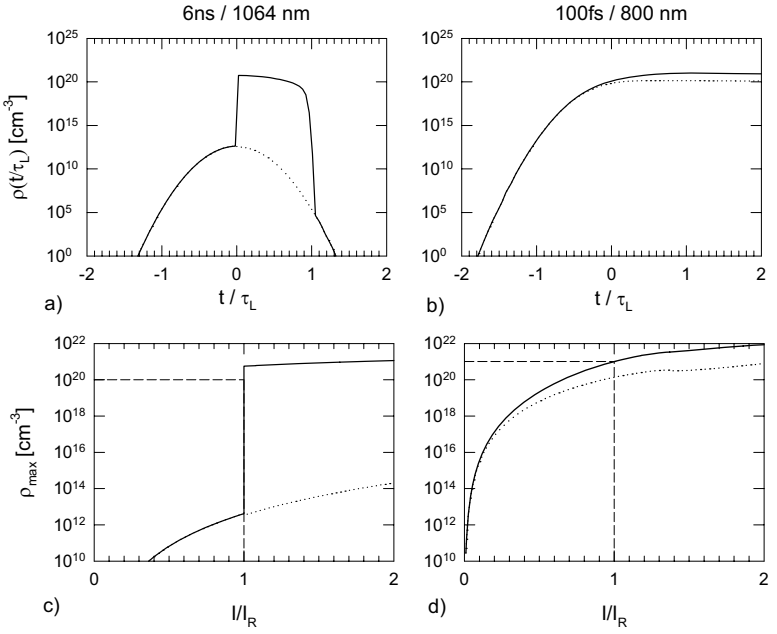

Figure 1. Top row: Evolution of the free-electron density during the laser pulse at the optical breakdown threshold for 6 ns, 1064 nm pulses and for 100-fs, 800-nm pulses. The time t is normalized with respect to the laser pulse duration τ_L. The contribution of multiphoton ionization to the total free-electron density is plotted as a dotted line. Bottom row: Maximum free electron density ρ_{max} achieved during the laser pulse as a function of irradiance, for the same laser parameters. The irradiance I is normalized with respect to the threshold irradiance I_{rate}. The threshold I_{rate} and the corresponding value of ρ_{max} are marked by dotted lines.

For a plane wave focused by a microscope objective, the focal region has an ellipsoidal shape. When long pulses are used for cell surgery and energy deposition is based on linear absorption, the possible spatial resolution is related to the temperature distribution in the focal region [1]. By contrast, for femtosecond laser pulses, the spatial resolution is defined by the free electron distribution, which, for 800 nm wavelength, is proportional to the 5^{th} power of the irradiance distribution. Due to nonlinear energy deposition, the achievable resolution is thus considerably better than the diffraction-limited optical resolution.

The lower end of the irradiance range useful for cell surgery is defined by the regime where the free electron density is still too low to cause any thermal or thermo-mechanical effects but sufficiently high to cause molecular bond breaking via resonant interactions between electrons of 3 -20 eV kinetic energy and biomolecules [5]. When long oscillator pulse series of ≈ 80 MHz repetition rate consisting of 10^4 to 10^6 pulses are employed, their accumulative chemical effects can lead to dissection.

The laser-induced temperature rise can be determined by calculating the volumetric energy density gained by the plasma during the laser pulse which, for femtosecond pulses, is simply given by the total number density ρ_{max} of the free electrons produced during the pulse multiplied by the mean energy gain of each electron. The mean energy gain of an electron is given by the sum of ionization potential and average kinetic energy. The temperature rise is related to the plasma energy density by the thermal constants of tissue (assumed to be equal to those of water). The results of the temperature calculations in figure 2 demonstrate that for repetition rates of several MHz, accumulative thermal effects are observed.

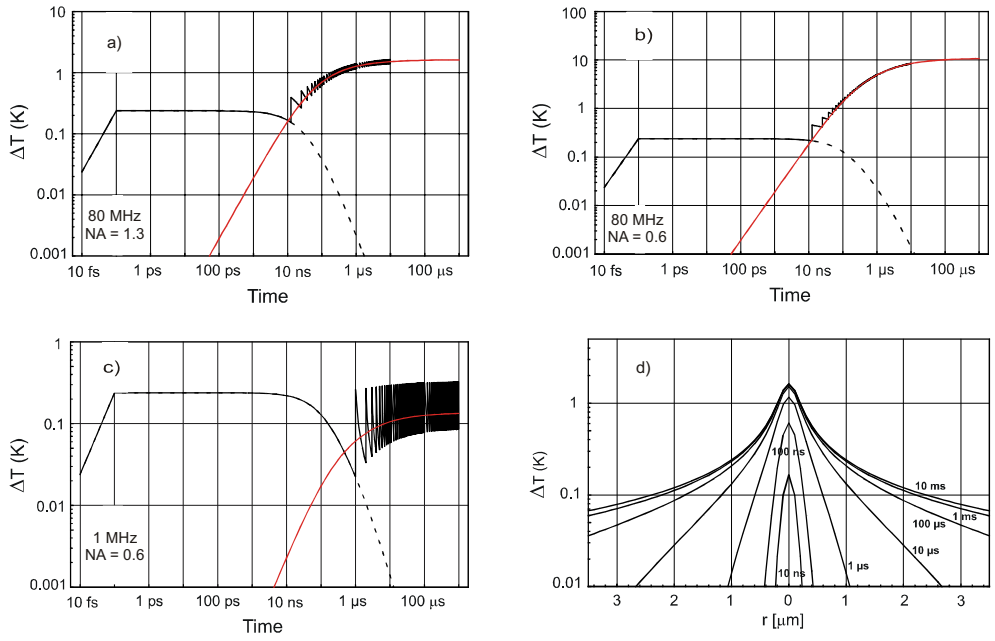

Figure 2. Temperature evolution at the center of the laser focus produced by a series of 800-nm, 100-fs pulses focused into water (a-c), and the corresponding temperature distribution (d). a) 80 MHz repetition rate, NA = 1.3; b) 80 MHz repetition rate, NA = 0.6; c) 1 MHz repetition rate, NA = 0.6, d) 80 MHz repetition rate, NA = 1.3. The volumetric energy density deposited per pulse was always assumed to be 1 Jcm^{-3} at the focus center. The dashed lines in a) – c) represent the temperature decay after a single pulse. For comparison, the temperature evolution during cw irradiation with the same average power as for pulsed irradiation is also shown.

For 80 MHz, the peak temperature after many pulses is up to 6.8 times higher than after a single pulse for NA = 1.3, and up to 45 times higher for NA = 0.6 (Figs. 2a, b). However, when the repetition rate is reduced to 1 MHz or smaller, heat accumulation disappears even for NA = 0.6 (Fig. 2c) because the narrow free electron distribution, which is the source of the heat deposition, leads to a very rapid heat diffusion. For NA = 1.3, the heat distribution exhibits a half-width in the submicrometer-range, as shown in Fig. 2d. Thermal effects are thus confined to a very small volume, even for long pulse series for which the thermal distribution resembles that of cw irradiation. However, it needs to be kept in mind that no purely thermal effects can be produced with femtosecond pulses, because due to the nonlinear absorption of the laser light heat generation is always mediated by the production of free electrons. For example, each pulse of a series leading to a final temperature of 100°C (at NA = 1.3) produces ≈ 2 Mil. free electrons. The thermal effects are, therefore, always accompanied and probably dominated by free-electron-mediated chemical effects.

For even larger irradiances, thermo-mechanical effects (bubble formation) come into play. When bubbles are formed during cell surgery with oscillator pulse series (≈ 80 MHz), they arise from accumulative chemical bond breaking and photothermolysis. They are long lasting, can grow to a fairly large size, and their appearance defines the upper limit of the useful parameter range for cell surgery with oscillator pulse series.

The situation is different in the single pulse regime ≤ 1 MHz, where no temperature accumulation occurs. Here bubbles are produced by thermo-elastically induced tensile stress. In femtosecond optical breakdown, laser pulse duration and thermalization time of the energy of the free electrons are much shorter than the acoustic transit time from the center of the focus to its periphery. Therefore, no acoustic relaxation is possible during the thermalization time, and the thermo-elastic stresses caused by the temperature rise stay confined in the focal volume, leading to a maximum pressure rise [6, 7]. Conservation of momentum requires that the stress wave emitted from the focal volume must contain both compressive and tensile components such that the integral of the stress over time vanishes. In water or biological cells, the tensile stress wave will cause the formation of a cavitation bubble when the rupture strength of the liquid is exceeded. For cell surgery, in the single pulse regime, the threshold for bubble formation defines the onset of disruptive mechanisms contributing to dissection.

To determine the evolution of the thermo-elastic stress distribution in the vicinity of the laser focus, we solved the three-dimensional thermo-elastic wave equation arising from the temperature distribution at the end of a single femtosecond laser pulse. The result is presented in Fig. 3.

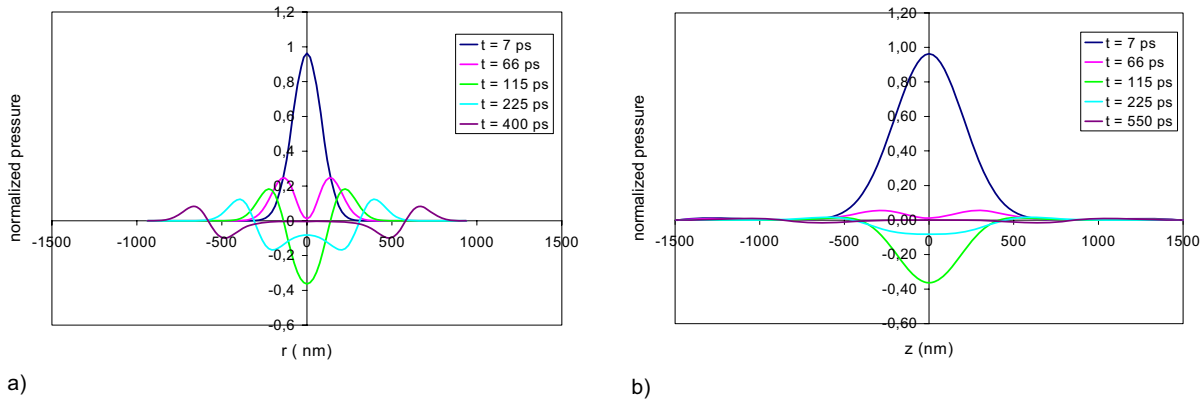

Figure 3. Stress distribution produced by a single femtosecond pulse of 800 nm wavelength focused into water (NA = 1.3) for various times after the release of the laser pulse, (a) in radial direction, and (b) in axial direction.

Because the region subjected to large tensile stress amplitudes is very small, the presence of inhomogeneous nuclei that could facilitate bubble formation is unlikely, and we have to consider the tensile strength of pure water to estimate the bubble formation threshold. We use the crossing of the "kinetic spinodal" as defined by Kiselev [8] as threshold criterion for bubble formation. For 20°C start temperature, this occurs at ΔT = 132°C, and p = - 71.5 MPa. For superthreshold pulse energies, the size of the bubble nucleus was identified with the extent of the region in which the negative pressure exceeds the kinetic spinodal limit. The bubble dynamics was then calculated by means of the Gilmore model, considering the tensile stress around the bubble and the vapor pressure inside the bubble as driving forces for the bubble expansion. An example for the bubble dynamics after a temperature rise from room temperature to 200°C is given in Fig. 4a, and the dependence between maximum bubble size and end temperature is presented in Fig. 4b. A comparison to experimental results on stress amplitudes, bubble formation thresholds and maximum bubble size can be found in Ref [1].

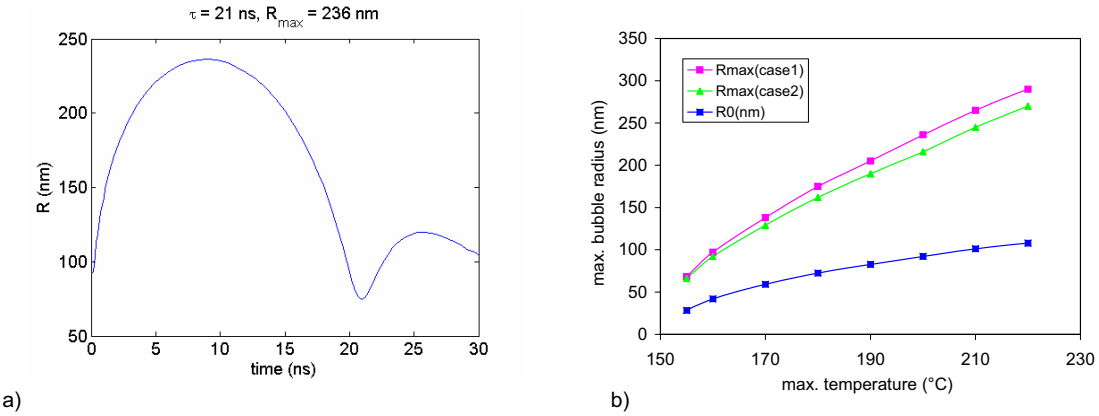

Figure 4. a) Radius time curve of the cavitation bubble produced by a single femtosecond laser pulse focused at NA = 1.3 that leads to a peak temperature rise of T_{max} = 200 °C at the focus center. b) Maximum bubble radius as a function of the maximum temperature achieved in the center of the focal volume, together with the radius of the nucleus, R_0. Cases 1 and 2 stand for isothermal and adiabatic conditions for the bubble content with respect to the surrounding liquid. In a), isothermal conditions are assumed.

The most prominent feature of the transient bubbles produced close to the threshold of femtosecond optical breakdown is their small size and short lifetime. The bubble radius amounts to only about 200 nm in water, and will be even smaller in a visco-elastic medium such as the cytoplasm. This makes a dissection mechanism associated with bubble formation compatible with intracellular nanosurgery, in contrast to nanosecond optical breakdown where the minimum bubble radius in water observed for NA = 0.9 was R_{max} = 45 µm [9]. The small bubble size corresponds to a small energy of only 53 femtoJoule of the expanded bubble for the case presented in Fig. 4a. The smallness of the bubble energy is largely due to the small energy content of the stress transient creating the bubble. For the case of Fig. 4a, the energetic conversion efficiency from heat into the thermo-elastic wave is only 0.46%, and the conversion efficiency from thermo-elastic energy into bubble energy is 6.8%.

The stress-confinement of the energy deposition in femtosecond laser induced material processing results in large compressive and tensile stress amplitudes already after a moderate temperature rise. Therefore, a temperature rise as little as 131.5 °C is sufficient for bubble generation in a liquid without any pre-existing nuclei. The low volumetric energy density required for thermoelastically induced cavity formation (only about 1/5 of the vaporization enthalpy) is a reason for the lack of thermal side effects in femtosecond laser dissection and the small conversion rate of laser energy into mechanical energy. Nevertheless, for sufficiently large pulse energies, bubble expansion and shock wave pressure can cause effects far beyond the focal volume that lead to cell death. To avoid unwanted side effects, irradiances should be used that are only slightly above the bubble formation threshold.

An overall view of physical effects induced by femtosecond laser pulses in comparison to experimental data on cell surgery is given in Fig. 5. It allows us to assess the working mechanisms in the different regimes of nanosurgery. Dissection at 80 MHz repetition rate is performed in the low-density plasma regime at pulse energies well below the optical breakdown threshold. It is mediated by free-electron-induced chemical decomposition (bond breaking) in conjunction with multiphoton-induced chemistry, and not related to heating or thermo-elastic stresses. When the energy is raised, long-lasting bubbles are produced by accumulative heating and tissue dissociation into volatile fragments that are usually un-wanted. By contrast, dissection with 1 kHz repetition rate is performed using about 10-fold larger pulse

energies and relies on thermo-elastically-induced formation of minute transient cavities with life times < 100 ns. Both modes of fs-laser nanoprocessing can achieve a 2-3 fold better precision than cell surgery using cw irradiation and enable manipulation at arbitrary locations [1].

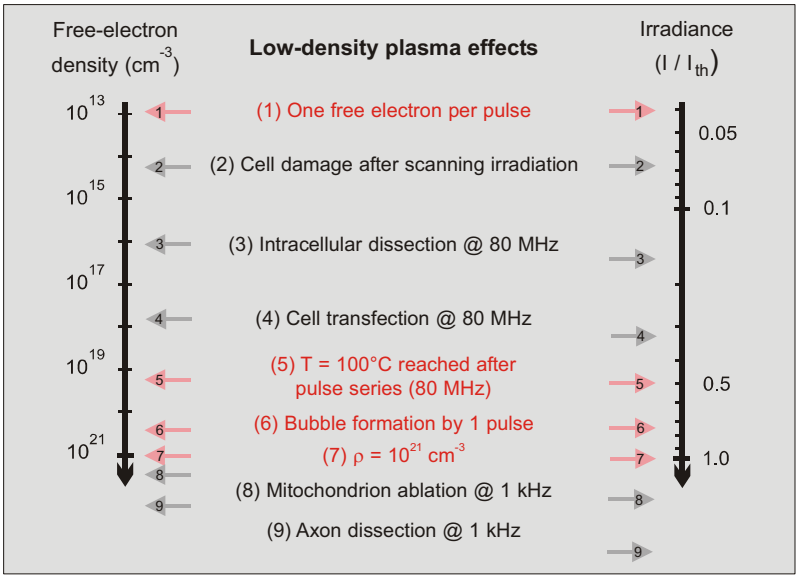

Figure 5. Overall view of physical breakdown phenomena induced by femtosecond laser pulses (marked in red), together with experimental damage, transfection and dissection thresholds for cells.

Besides for nanoprocessing of biological materials, femtosecond laser induced plasmas can also be used to modify other transparent materials and enable the generation of photonic elements in bulk glass and fused silica. The process of plasma generation and void formation in the bulk of dielectric like fused silica and glass resembles the process in water, and the methods developed in our study can also be applied to solid dielectric. However, differences in the band gap energy and material properties will lead to somewhat larger threshold values for chemical and thermo-mechanically induced changes in solids compared to aqueous media.

References

[1] Vogel A, Noack J, Hüttman G and Paltauf G 2005 *Appl. Phys. B* **81,** 1015
[2] Mao SS, Quéré F, Guizard S, Mao X, Russo RE, Petite G and Martin P 2004 *Appl. Phys. A* **79**, 1695
[3] Stuart BC, Feit MD, Hermann S, Rubenchik AM, Shore BW and Perry MD 1996 *Phys. Rev. B* **53**, 1749
[4] Joglekar AP, Liu H, Meyhöfer E, Mourou G and Hunt AL 2004 *Proc. Nat. Acad. Sci.* **101**, 5856
[5] Boudaiffa B, Cloutier P, Hunting D, Huels MA and Sanche L 2000 *Science* **287** 1658
[6] Vogel A and Venugopalan V 2003 *Chem. Rev.* **103** 577
[7] Paltauf G and Dyer P 2003 *Chem. Rev.* **103** 487
[8] Kiselev SB 1999 *Physica A* **269** 252
[9] Venugopalan V, Guerra A, Nahen K and Vogel A 2002 *Phys. Rev. Lett.* **88** 078103